Creating nitrogen–vacancy ensembles in diamond for coupling with flux qubit*

Ya-Rui Zheng(郑亚锐), Jian Xing(邢健), Yan-Chun Chang(常彦春), Zhi-Guang Yan(闫智广), Hui Deng(邓辉), Yu-Lin Wu(吴玉林), Li Lü(吕力), Xin-Yu Pan(潘新宇), Xiao-Bo Zhu(朱晓波)†, and Dong-Ning Zheng(郑东宁)‡

Institute of Physics, Chinese Academy of Sciences, Beijing 100190, *China*

(Received 4 November 2016; revised manuscript received 24 November 2016; published online 10 January 2017)

Hybrid quantum system of negatively charged nitrogen–vacancy (NV^-) centers in diamond and superconducting qubits provide the possibility to extend the performances of both systems. In this work, we numerically simulate the coupling strength between NV^- ensembles and superconducting flux qubits and obtain a lower bound of 10^{16} cm^{-3} for NV^- concentration to achieve a sufficiently strong coupling of 10 MHz when the gap between NV-ensemble and flux qubit is 0. Moreover, we create NV^- ensembles in different types of diamonds by $_{14}N^+$ and $_{12}C^+$ ion implantation, electron irradiation, and high temperature annealing. We obtain an NV^- concentration of 1.05×10^{16} cm^{-3} in the diamond with 1-ppm nitrogen impurity, which is expected to have a long coherence time for the low nitrogen impurity concentration. This shows a step toward performance improvement of flux qubit-NV^- hybrid system.

Keywords: flux qubit, nitrogen–vacancy center, hybrid quantum system

PACS: 03.67.Lx, 81.05.ug, 85.25.Cp **DOI:** 10.1088/1674-1056/26/2/020305

1. Introduction

Superconducting quantum circuits became one of the most promising systems to build a quantum computer due to its rapid progress in recent years. It has great potential in scaling up[1] and design flexibility.[2–5] However, superconducting qubits still suffer several difficulties, such as inability of long distance quantum teleportation and lack of long life time memory. On the other hand, ultra-long coherence time approaching to 1 s has been demonstrated in negatively charged nitrogen–vacancy (NV^-) centers in diamond.[6] Moreover, NV^- centers have both optical and microwave energy levels. This makes NV^- centers a suitable candidate for optics-microwave quantum interface[7–10] which would allow optical quantum teleportation between distant distributed superconducting qubits. Hybrid quantum systems of NV^- and superconducting qubits[11] would largely extend the performances of both independent systems.

Creating NV^- ensemble in diamond has been widely investigated.[12–14] Hybrid systems of superconducting qubits and NV^- centers have also been experimentally demonstrated.[15,16] However, increasing the coherence time of NV^- ensembles while maintaining a sufficiently strong coupling strength remains a challenge. In the previous experiments, relatively high concentration of NV^- ensembles were used to achieve a sufficiently strong coupling strength. Dominant decoherence sources in such samples include a large quantity of P1 centers (i.e., a nitrogen atom substituting a carbon atom) and the interaction between NV^- centers.[17] A natural solution to these problems is to reduce the concentration of P1 centers and NV^- centers in the diamond. However, this will reduce the coupling strength between NV^- ensemble and superconducting qubits.

Here, we numerically simulate the coupling strength between NV^- ensemble and a superconducting flux qubit and obtain a lower bound of 10^{16} cm^{-3} for NV^- concentration to achieve a sufficiently strong coupling of 10 MHz. Then we create NV^- ensemble in diamonds by three different ways of electron irradiation, $_{14}N^+$ and $_{12}C^+$ ion implantation, respectively.

We obtain an NV^- concentration of 1.05×10^{16} cm^{-3} in diamond with a relatively low nitrogen impurity of 1 ppm. This shows the possibility to improve the coherence time of flux qubit-NV^- hybrid system.

2. Theory

The Hamiltonian of NV^- center[18] can be described as

$$H_{\rm NV} = hDS_z^2 + hE\left(S_x^2 - S_y^2\right) + hg_{\rm e}\mu_{\rm B}\boldsymbol{B}\cdot\boldsymbol{S}, \qquad (1)$$

where $S_{x,y,z}$ are the components of spin-one operator $\boldsymbol{S}$; z is the direction of NV axis; D is the zero field splitting (2.878 GHz); E is the strain induced splitting (<10 MHz); $g_{\rm e}=2$ is the

*Project supported in part by the National Natural Science Foundation of China (Grant Nos. 91321208, 11574386, 11374344, and 11574380), the National Basic Research Program of China (Grant Nos. 2014CB921401 and 2016YFA0300601), and the Strategic Priority Research Program of the Chinese Academy of Sciences (Grant No. XDB07010300).

†Corresponding author. E-mail: xbzhu16@ustc.edu.cn

‡E-mail: dzheng@iphy.ac.cn

© 2017 Chinese Physical Society and IOP Publishing Ltd

Landé factor of NV^- center; $\mu_B = 14$ MHz/mT is the Bohr magneton; h is the Planck's constant.

Superconducting flux qubit is a superconducting loop broke by three Josephson junctions (or replace the smallest junction by a direct current (DC) superconduccting quantum interference device (SQUID) for gap tunability). When biasing the loop near half flux quantum, flux qubit can be approximated as an effective two-level system described by the Hamiltonian[2]

$$H_{FQ} = \frac{h}{2}(\Delta\sigma_z + \epsilon\sigma_x), \tag{2}$$

where $\sigma_{x,z}$ are Pauli matrices with σ_x whose eigenstates correspond to the clockwise and anticlockwise persistent-current states;

$$h\varepsilon = 2I_p\left[\Phi_{ex} - \left(n + \frac{1}{2}\Phi_0\right)\right]$$

is the energy bias; I_p is the persistent current; Φ_{ex} is the external magnetic flux; $\Phi_0 = h/2e$ is the flux quantum; Δ is tunneling splitting.

The interaction Hamiltonian between flux qubit and NV^- ensembles[11] is

$$H_{Int} = h\sum_i^N g_e\mu_B\sigma_x \boldsymbol{B}_i \cdot \boldsymbol{S}_i, \tag{3}$$

where $\boldsymbol{S}_i$ is the spin-one operator of the i-th NV^- center and $\boldsymbol{B}_i$ is the magnetic field generated by the persistent current of flux qubit at the position of the i-th NV^- center.

For simplicity, we assume that $\boldsymbol{B}$ and E are small enough to be neglected in Eq. (1). When flux qubit coupled with NV^- ensembles at degenerate point, where $\epsilon = 0$, the total Hamiltonian can be simplified into

$$H_{Tot} = \frac{h}{2}\Delta\sigma_z + h\sum_i^N \left(DS_{z,i}^2 + g_e\mu_B\sigma_x \boldsymbol{B}_i \cdot \boldsymbol{S}_i\right). \tag{4}$$

By making the rotating wave approximation, we have

$$H_{Tot} = \frac{h}{2}\Delta\sigma_z + h\sum_i^N \left[DS_{z,i}^2 + g_e\mu_B B_{\perp,i}(\sigma_+ S_{-,i} + \sigma_- S_{+,i})\right], \tag{5}$$

where $\sigma_\pm$ are the rising and lower operators for the flux qubit,

$$S_+ = \frac{1}{\sqrt{2}}(|1\rangle\langle 0| + |-1\rangle\langle 0|),$$
$$S_- = \frac{1}{\sqrt{2}}(|0\rangle\langle 1| + |0\rangle\langle -1|)$$

are the effective rising and lower operators for the NV^- centers and $B_{\perp,i}$ is the component of magnetic field generated by the persistent current in flux qubit that is perpendicular to the NV axis. By defining collective operators

$$b = \frac{1}{G}\sum_i^N g_e\mu_B B_{\perp,i} S_{-,i}, \tag{6}$$

$$b^\dagger = \frac{1}{G}\sum_i^N g_e\mu_B B_{\perp,i} S_{+,i}, \tag{7}$$

we can consider the NV^- ensembles as a generalized harmonic oscillator coupled to the flux qubit with the coupling strength

$$G = g_e\mu_B\sqrt{\sum_i^N B_{\perp,i}^2}.$$

Replacing the summation with integral for large scale of ensembles with NV^- concentration ρ, we derive the coupling strength as

$$G = g_e\mu_B\sqrt{\int B_\perp^2 \rho\, dV}. \tag{8}$$

Note that NV^- centers have 4 possible directions in the diamond crystal. We assume that NV^- centers in all directions have the same distribution in the diamond crystal. By a simple calculation, we can summate the coupling strengths for all possible directions and obtain

$$G = \sqrt{\frac{2}{3}}g_e\mu_B\sqrt{\int B^2\rho\, dV}. \tag{9}$$

3. Numerical simulation

Here we aim at finding a lower bound for NV^- concentration to achieve a sufficiently strong coupling between NV^- ensembles and flux qubit, that is, a coupling strength far larger than the decay rate of both systems. Flux qubit with coherence time larger than 1 μs is now available experimentally.[19] NV- ensembles with coherence time $\sim$ μs is also available.[20] Thus we chose a lower bound for the coupling strength to be G= 10 MHz, which is about 10 times large than the decay rates of both systems. According to Eq. (9), we can obtain the lower bound for NV^- concentration as

$$\rho = \frac{3G^2}{2g_e^2\mu_B^2} \times \frac{1}{\int B^2\, dV}, \tag{10}$$

where $\int B^2\, dV$ can be derived by numerically simulating magnetic field generated by the persistent current in the flux qubit loop.

Figure 1(a) shows an SEM image of a flux qubit device which follows the design and fabrication process as described in Ref. [21]. The red part is the qubit loop. By using different junction parameters, the persistent current I_p in the main qubit loop can be varied from 100 nA to 1 μA. Figure 1(b) shows a simulation schematic of the hybrid system. The red part is the qubit loop the same as in Fig. 1(a). The box above the flux qubit is the NV^- ensemble. We simulate the magnetic field distribution by finite element analysis. Figure 1(c) shows the simulated result. We calculate gap dependence of NV^- concentration which is required to achieve a 10-MHz coupling strength for I_p = 300 nA and I_p = 500 nA, where the gap is the distance between bottom surface of NV^- ensemble and top surface of flux qubit. The simulated results give a lower bound of 9.96×10^{15} cm^{-3} for NV^- concentration when the I_p is 500 nA and there is no gap between NV^- ensemble and flux qubit.

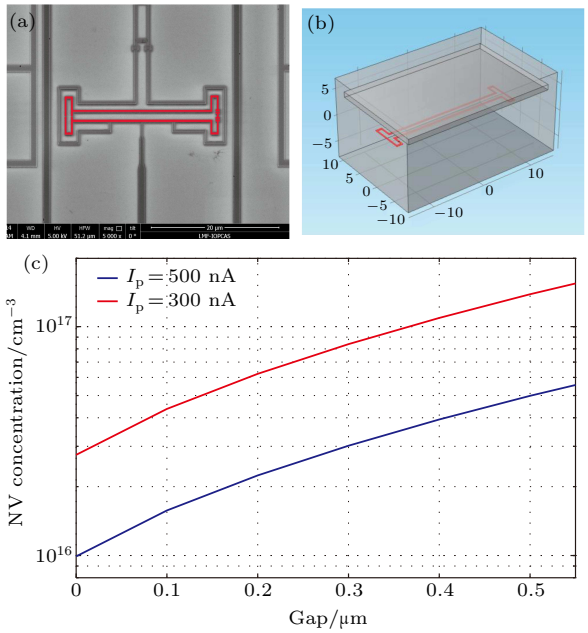


Fig. 1. (color online) (a) SEM image of a flux qubit device. The red part is the flux qubit loop. The width and thickness of the wire are 300 nm and 80 nm, respectively. By using different junction parameters, the persistent current I_p in the main loop can vary from 100 nA to 1 μA. (b) Schematic diagram for the coupling strength simulation. The red part is the flux qubit loop, which has the same size as in panel (a). The box above the flux qubit loop is the NV^- ensemble. We simulate the magnetic field distribution by finite element analysis. (c) Simulated results. We calculate gap dependent NV^- concentration required to achieve a 10-MHz coupling strength for $I_p = 300$ nA and $I_p = 500$ nA, where gap is the distance between bottom surface of NV^- ensemble and top surface of flux qubit. The simulated result gives a lower bound of 9.96×10^{15} cm^{-3} for NV^- concentration when I_p is 500 nA and there is no gap between NV^- ensemble and flux qubit.

To confirm our simulated result, we numerical calculate the coupling strength between flux qubit and NV^- ensemble in Ref. [16], where the persistent current I_p is 300 nA, the NV^- concentration is 1.1×10^{18} cm^{-3}, the distance between flux qubit and NV^- ensemble is 1 μm, and the coupling strength is measured to be 35 MHz. The simulated result is 10 MHz. There are two most possible reasons for the difference between simulated and experimental result: (i) the distance between flux qubit and NV^- ensemble is difficult to measure; (ii) in high NV^- concentration sample, NV^- centers will absorb and scatter photoluminescence from other NV^- centers and reduce the total photoluminescence, hence reduce the estimated NV^- concentration. Recently, we also coupled a gradient flux qubit to NV^- ensemble, where the persistent current I_p is 1.28 μA, the NV^- concentration is measured to be 8.8×10^{17} cm^{-3} and the distance between NV^- sample and flux qubit is estimated to be 600 nm. The simulated and experimental coupling strength are 33.5 MHz and 56.5 MHz, respectively. This shows that our simulated results are quite compatible with the experimental result.

4. Experiment

We create the NV^- centers in the diamond by $_{14}N^+$ and $_{12}C^+$ ion implantation, electron irradiation and high temperature annealing as shown in Table 1. The diamond sample used in our experiment was fabricated commercially by Element-6 through using either chemical-vapor deposition (CVD) or high-pressure high-temperature (HPHT) synthesis. The initial nitrogen concentration was given as about 1 ppm (1 ppm corresponds to 1.76×10^{17} cm^{-3} in diamond) and 200 ppm for CVD samples and HPHT sample, respectively. Each sample was annealed several times to check the saturated annealing time. After each annealing process, all samples were boiled in a 1:1:1 mixture of sulfuric, nitric, perchloric acids for 3 h to remove any graphitic contamination at the surface.

Optical characterization was performed by using confocal microscopy at room temperature. Light from a commercial solid-state 532-nm laser was used to excite an optical transition associated with the NV^- center $_3E$ excited-state manifold. A microscope objective was used to focus the light into a submicron spot and collect the photoluminescence (PL) from NV^- centers. A 650-nm long-pass filter filtered out the

Table 1. List of samples and the main results. Initial nitrogen concentration, [N], is given as specified by Element-6. Each sample is annealed several times to check the saturated annealing time. After each annealing process, samples are boiled in a 1:1:1 mixture of sulfuric, nitric, perchloric acids for 3 hours to remove any graphitic contamination at the surface.

No.	Synthesis	[N]/ppm	Radiation	Energy/MeV	Dose/cm^{-2}	Annealing process	Final NV^-/cm^{-3}
S1	CVD	~ 1	$_{14}N^+$	0.5	2.5×10^{12}	900 °C 3 h, 900 °C 3 h, 1000 °C 12 h, 1000 °C 48 h	9.10×10^{14}
S2	CVD	~ 1	$_{14}N^+$	0.5	2.5×10^{13}	900 °C 3 h, 900 °C 3 h, 1000 °C 12 h, 1000 °C 48 h	5.79×10^{15}
S3	CVD	~ 1	$_{14}N^+$	0.5	2.5×10^{14}	900 °C 3 h, 900 °C 3 h, 1000 °C 12 h, 1000 °C 48 h	9.08×10^{15}
S4	HPHT	~ 200	$_{12}C^+$	0.4	3×10^{13}	1000 °C 72 h	3.78×10^{16}
S5	HPHT	~ 200	$_{12}C^+$	0.4	3×10^{14}	1000 °C 72 h	1.91×10^{17}
S6	CVD	~ 1	e	1.5	1×10^{17}	1000 °C 24 h, 1000 °C 48 h	7.71×10^{15}
S7	CVD	~ 1	e	1.5	3×10^{17}	1000 °C 24 h, 1000 °C 48 h	9.23×10^{15}
S8	CVD	~ 1	e	1.5	1×10^{18}	1000 °C 24 h, 1000 °C 48 h	1.05×10^{16}
S9	HPHT	~ 200	e	1.5	1×10^{17}	1000 °C 24 h, 1000 °C 48 h	1.85×10^{16}
S10	HPHT	~ 200	e	1.5	3×10^{17}	1000 °C 24 h, 1000 °C 48 h	6.95×10^{16}
S11	HPHT	~ 200	e	1.5	1×10^{18}	1000 °C 24 h, 1000 °C 48 h	1.70×10^{17}

reflected laser light. The collected photoluminescence was detected by using a single-photon-counter. The NV^- concentration C is estimated for $C = P_E/(P_S V)$, where P_E and P_S are the intensities of the photoluminescence of NV^- ensemble and single NV^- center, respectively, V is the effect volume of the detected region, which can be determined by scanning the image of a single NV^- center. In our experiment, P_S and V were measured to be 4×10^4 counts per second and 0.7 μm^{-3}, respectively.

5. Results and discussion

Figure 2 shows the plots of NV concentration versus total annealing time. The NV concentrations of samples S2 and S3 are increased at least by 100% after annealing for a total of 66 hours as compared with annealing for 3 hours. And the concentrations of samples S6–S11 are increased by about 20% after annealing for a total of 72 hours as compared with annealing for 24 hours. This suggests that there is a large quantity of vacancies that neither recombine with each other nor form NV centers after annealing for 24 hours. An annealing process longer than 72 hours would be useful to increase the NV concentration and reduce the defects in the diamond crystal.

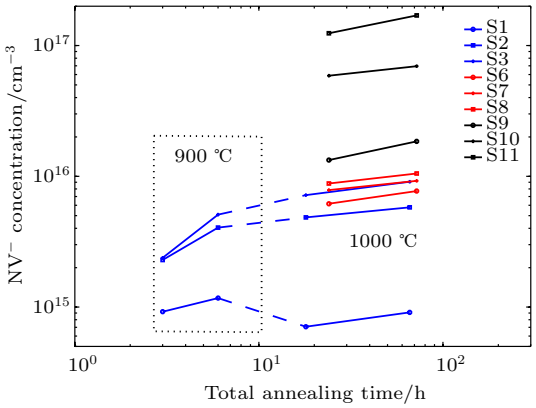


Fig. 2. (color online) Plots of NV concentration versus total annealing time. Datum points in dash line box are measured after annealing at 900 °C, which are for first two annealing processes of S1–S3 as shown in the Table 1. Other datum points are measured after annealing at 1000 °C. Almost all the NV concentrations, expect S1, increase as the annealing time increases. The reason why S1 does not increase with the annealing time is unknown for the time being.

Figure 3 shows the plots of NV^- concentration versus electron irradiation dose. In samples S9–S11, which have initial nitrogen impurity concentrations of about 200 ppm, NV^- concentrationis roughly proportional to the irradiation dose. In samples S6–S8, whose initial nitrogen impurity concentrations are about 1 ppm, the NV^- concentrations increase only about 30% as the irradiation dose increases 9 times. This suggests that the NV^- concentration is saturated at these doses for single electron irradiation. Moreover, sample S8 has a final NV^- concentration of 1.05×10^{16} cm^{-3}, reaching the lower bound we estimated previously to achieve a sufficiently strong coupling between flux qubit and NV^- ensemble.

The highest conversion efficiencies from nitrogen impurities to NV^- centers for 1-ppm sample and 200-ppm sample are 6% and 1%, respectively. The low conversion efficiency in 200-ppm sample is due to the lack of vacancies. A natural solution is used to increase the electron irradiation dose. This will increase the vacancies created by irradiation. In 1-ppm sample, NV^- concentration is saturated. The possible more efficient way is to repeat the electron irradiation and high temperature annealing process several turns or irradiate the sample at high temperature.

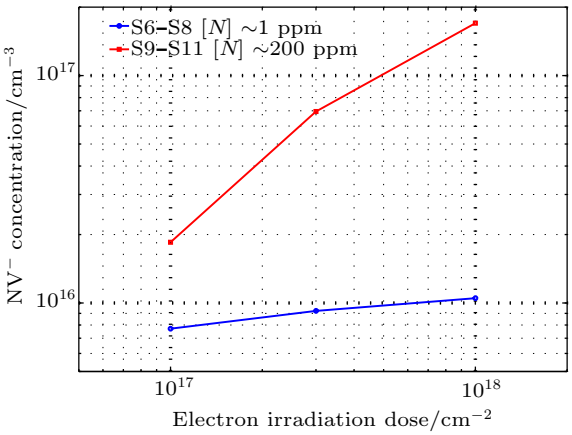


Fig. 3. (color online) Plots of NV concentration versus electron irradiation dose. In samples S9–S11, which have initial nitrogen impurity concentrations of about 200 ppm, NV concentrations are roughly proportional to the irradiation dose. In samples S6–S8, whose initial nitrogen impurity concentrations are about 1 ppm. The NV concentration increases only about 30% as the irradiation dose increases 9 times. This suggests that the NV concentration is saturated at these doses for single electron irradiation.

6. Summary

We numerically simulate the coupling strength between flux qubit and NV^- ensembles and derive a lower bound of NV^- concentration of about 1×10^{16} cm^{-3} to achieve a sufficiently strong coupling between flux qubit and NV^- ensemble. Moreover, we create NV^- centers in diamond crystal samples by ion implantation, electron irradiation and high temperature annealing. Finally, we obtain an NV^- concentration of 1.05×10^{16} cm^{-3} in a CVD synthesized diamond sample with $\sim$ 1-ppm initial nitrogen impurity, which is expected to have longer NV^- coherence time than diamond with higher nitrogen impurity. This shows an important step toward improving the performance of the hybrid system composed of flux qubit and NV^- ensemble.

Acknowledgment

The authors thank Chengchun Tang, Haifang Yang, Aizi Jin and Junjie Li for help in the micro-fabrication of samples.

References

[1] Kelly J, Barends R and Fowler A G, *et al.* 2015 *Nature* **519** 66

[2] Mooij J E, Orlando T P, Levitov L, Tian L, van der Wal C H and Lloyd S 1999 *Science* **285** 1036
[3] Nakamura Y, Pashkin Y A and Tsai J S 1999 *Nature* **398** 786
[4] Martinis J, Nam S, Aumentado J and Urbina C 2002 *Phys. Rev. Lett.* **89** 117901
[5] Koch J, Yu T M, Gambetta J, Houck A A, Schuster D I, Majer J, Blais A, Devoret M H, Girvin S M and Schoelkopf R J 2007 *Phys. Rev. A* **76** 042319
[6] Bar-Gill N, Pham L M, Jarmola A, Budker D and Walsworth R L 2013 *Nat. Commun.* **4** 1743
[7] O'Brien C, Lauk N, Blum S, Morigi G and Fleischhauer M 2014 *Phys. Rev. Lett.* **113** 063603
[8] Williamson L A, Chen Y H and Longdell J J 2014 *Phys. Rev. Lett.* **113** 203601
[9] Xia K Y and Twamley J 2015 *Phys. Rev. A* **91** 042307
[10] Pei P, Huang H F, Guo Y Q and Song H S 2016 *Chin. Phys. Lett.* **33** 020301
[11] Marcos D, Wubs M, Taylor J M, Aguado R, Lukin M D and Sørensen A S 2010 *Phys. Rev. Lett.* **105** 210501
[12] Acosta V M, Bauch E, Ledbetter M P, Santori C, Fu K M C, Barclay P E, Beausoleil R G, Linget H, Roch J F, Treussart F, Chemerisov S, Gawlik W and Budker D 2009 *Phys. Rev. B* **80** 115202
[13] Fávaro de Oliveira F, Momenzadeh S A, Antonov D, Fedder H, Denisenko A and Wrachtrup J 2016 *Physica Status Solidi (a)* **213** 2044
[14] Schwartz J, Aloni S, Ogletree D F and Schenkel T 2012 *New J. Phys.* **14** 043024
[15] Kubo Y, Grezes C, Dewes A, Umeda T, Isoya J, Sumiya H, Morishita N, Abe H, Onoda S, Ohshima T, Jacques V, Dréau A, Roch J F, Diniz I, Auffeves A, Vion D, Esteve D and Bertet P 2011 *Phys. Rev. Lett.* **107** 220501
[16] Zhu X B, Saito S, Kemp A, Kakuyanagi K, Karimoto S, Nakano H, Munro W J, Tokura Y, Everitt M S, Nemoto K, Kasu M, Mizuochi N and Semba K 2011 *Nature* **478** 221
[17] Hanson R, Dobrovitski V V, Feiguin A E, Gywat O and Awschalom D D 2008 *Science* **320** 352
[18] Neumann P, Kolesov R, Jacques V, Beck J, Tisler J, Batalov A, Rogers L, Manson N B, Balasubramanian G, Jelezko F and Wrachtrup J 2009 *New J. Phys.* **11** 013017
[19] Stern M, Catelani G, Kubo Y, Grezes C, Bienfait A, Vion D, Esteve D and Bertet P 2014 *Phys. Rev. Lett.* **113** 123601
[20] Grezes C, Julsgaard B, Kubo Y, MaWL, Stern M, Bienfait A, Nakamura K, Isoya J, Onoda S, Ohshima T, Jacques V, Vion D, Esteve D, Liu R B, Mølmer K and Bertet P 2015 *Phys. Rev. A* **92** 020301
[21] Deng H, Wu Y L, Zheng Y R, Akhtar N, Fan J, Zhu X B, Li J, Jin Y R and Zheng D N 2015 *IEEE Trans. Appl. Superconductivity* **25** 1